# Flexible and transparent films produced from cellulose nanowhisker reinforced agarose

*Reda M. Felfel[1,2•*], Kazi M. Zakir Hossain[1•*], Sumaya F. Kabir[1], Soon L. Yee[3], Ifty Ahmed[1] and David M. Grant[1]*

[1]Advanced Materials Research Group, Faculty of Engineering, University of Nottingham, UK

[2]Physics Department, Faculty of Science, Mansoura University, Mansoura, Egypt

[3]Nano and Advanced Materials Institute Limited, Hong Kong

• Shared first authorship

***Corresponding authors**: Reda M. Felfel, reda.felfel@nottingham.ac.uk and Kazi M. Zakir Hossain, ezzzh@exmail.nottingham.ac.uk

## Research Highlights

- Never-dried CNWs and Agarose were utilised to produce transparent and flexible nanocomposite films.
- The nanocomposites films maintained more than 84% optical transparency.
- The crystallinity of the nanocomposite films increased with the addition of CNWs.
- A significant increase in mechanical and thermomechanical properties of the nanocomposites was obtained.
- Incorporation of CNWs led to reduction in the swelling rate of the nanocomposite.

## Abstract

Transparent and flexible nanocomposite films with a range of Agarose to Cellulose Nano-Whisker (CNW) ratios were produced using never-dried CNWs. The incorporation of never-dried CNWs within Agarose played an important role in the surface roughness (Ra 7 to 15 nm) and light transparency of the films (from 84 to 90%). Surface induced crystallisation of Agarose by CNWs was also found with increasing percentage of crystallinity (up to 79%) for the nanocomposite films, where CNW acted as nucleating sites. The enhanced tensile strength (*ca.* 30% increase) and modulus (*ca.* 90% increase) properties of the nanocomposite



This is a peer-reviewed, accepted author manuscript of the following research article: Felfel, R. M., Hossain, K. M. Z., Kabir, S. F., Liew, S. Y., Ahmed, I., & Grant, D. M. (2018). Flexible and transparent films produced from cellulose nanowhisker reinforced agarose. Carbohydrate Polymers, 194, 328-338. https://doi.org/10.1016/j.carbpol.2018.04.005

films compared to the control Agarose film indicated the effectiveness of the nanowhiskers incorporation. The storage modulus of the nanocomposite films increased also to be tripled Agarose alone as the CNWs content reached 43%. The swelling kinetics of the nanocomposites revealed that addition of CNWs reduced the long-term swelling capacity and swelling rate of the nanocomposite.

***Keywords:*** *Cellulose nanowhiskers, agarose, transparency, crystallinity, tensile properties, swelling kinetics.*

## Introduction

Polymer nanocomposites consist of at least one of the phases with a dimension of nanoscale range (<100 nm) dispersed in a continuous polymer matrix. Polymer nanocomposites have been heavily studied for a wide range of uses, from water treatment (Pandey, Shukla, & Singh, 2017) and energy storage (Riggs et al., 2015) to biomedical applications (Zare & Shabani, 2016), due to their unique mechanical, chemical, optical, thermal, electrical and biological properties (Camargo, Satyanarayana, & Wypych, 2009; Müller et al., 2017). Different methods have been developed to produce polymer nanocomposites such as melt mixing (Jordan, Jacob, Tannenbaum, Sharaf, & Jasiuk, 2005), solution casting/evaporation (Kargarzadeh et al., 2017), in situ polymerisation (Jordan et al., 2005) and sol-gel process (Müller et al., 2017). Selection between those techniques is mainly dependent on the polymer matrix.

Highly transparent polymer nanocomposites have been developed utilising various nanoparticles, e.g. quantum dot (C. Liu et al., 2017), silver nanowires, graphene oxide (Tematio, Fosso, Krähenbühl, & Schintke, 2016), zinc sulphate (Cheng et al., 2008), gold (Ehlert, Stegelmeier, Pirner, & Förster, 2015; Khalil, Homaeigohar, Häußler, & Elbahri, 2016), nanoclay (Aulin, Salazar-Alvarez, & Lindstrom, 2012), silica and silica-titania (Y.-Q. Li, Fu, Yang, & Mai, 2008), for different applications including gamma scintillation, medical (C. Liu et al., 2017), photovoltaics, printed organic electronics, optical and optoelectronic devices (Tematio et al., 2016). The high transparency of highly-loaded (up to 60 w%) nanocomposites was achieved by using in situ polymerization process (Althues, Simon, & Kaskel, 2007; Cheng et

al., 2008; C. Liu et al., 2017) and/or surface modification of the nanoparticles (Bin, Sugihara, Elim, Adschiri, & Kaino, 2011; Dang et al., 2014).

Agglomeration and a lack of dispersion of the nanoparticles remain as one of the main challenges in manufacturing polymer nanocomposites (Y. Liu et al., 2015). Absence of chemical interaction between the phases and smaller aspect ratio nanofillers can lead to limited mechanical properties of the nanocomposites produced (Qiang, Chunfang, JianZun, & Yuan, 2004). It is expected that the mechanical properties of the nanocomposites will increase by increasing the aspect ratio of the nanofiller (Cipiriano et al., 2007; Yu et al., 2017). Therefore, carbon nanotubes (Sahoo, Rana, Cho, Li, & Chan, 2010), cellulose nanowhiskers (CNWs) (Santamaria-Echart et al., 2017) and hydroxyapatite nanorods (Yang et al., 2017) would be anticipated to have significantly greater reinforcement effects than nanospheres for example (Hassanabadi & Rodrigue, 2014). Several attempts have been made to enhance the dispersion and chemical interaction between polymer matrix and nanoparticles via surface treatment of the nanoparticles (D. Liu, Pourrahimi, Olsson, Hedenqvist, & Gedde, 2015). The nanoparticles show good dispersion in solution such as water, however then commonly tend to agglomerate during drying either at room temperature, in ovens or using freeze drying processes (Rahman, Vejayakumaran, Sipaut, Ismail, & Chee, 2008). Consequently, using an alternative process involving nanoparticle suspensions could result in enhanced nanoparticles distribution within polymer matrices, thus leading to advanced mechanical properties.

CNWs are usually produced via acid hydrolysis of cellulose based raw materials such as cotton, wood and ramie (George & Sabapathi, 2015; Trache, Hussin, Haafiz, & Thakur, 2017; Xu et al., 2013). Their aspect ratio, ratio of length to diameter or width, varies from 2 to 200 depending on the source of the cellulose and acid hydrolysis parameters (types of acid, hydrolysis period and temperature) (Trache et al., 2017). CNWs were selected here as a reinforcement due to their greater theoretical tensile strength, *ca.* 7.6 GPa, compared to Kevlar fibres and steel wires (Trache et al., 2017). Their elastic modulus was determined using AFM and found to be approximately 150 GPa (Iwamoto, Kai, Isogai, & Iwata, 2009; Trache et al., 2017). Due to these mechanical properties and aspect ratio, CNWs could be regarded as ideal natural, renewable, cytocompatible and biodegradable nanomaterials (Trache et al., 2017). Geometry and microstructure of CNWs were reported to be strongly influenced by the drying conditions

employed (Khoshkava & Kamal, 2014). CNWs whilst suspended in water, showed a needle shaped morphology with average length of *ca.* 170 nm and 15 nm diameter (George & Sabapathi, 2015). Small spherical shapes have been obtained by spray drying of CNWs, whilst freeze drying yielded larger flake shaped samples (Khoshkava & Kamal, 2014) showing the aspect ratio and morphology of CNWs can be significantly affected by the drying process. CNWs also tend to agglomerate and form large flakes at the drying step of production due to their high surface energy and specific surface area (Khoshkava & Kamal, 2014). Therefore, it would be considered highly desirable to use CNWs in suspension form to maintain their unique nano morphologies.

Agarose is a natural, biocompatible polymer obtained from seaweed (Cao, Gilbert, & He, 2009). Agarose has been heavily utilised in hydrogel form for electrophoresis purposes (Corthell, 2014). It has also been investigated as 3D porous constructs for biomedical applications such as regeneration of cartilage (Gadjanski, Yodmuang, Spiller, Bhumiratana, & Vunjak-Novakovic, 2013), wound healing (Awadhiya, Tyeb, Rathore, & Verma, 2017) and neural tissue engineering (Cao et al., 2009). Very few studies have explored the properties of agarose in dried thin sheet form. A highly transparent film of agarose can be obtained by drying the hydrogel at room temperature (Z. Wang et al., 2010 a; Z. Wang et al., 2010 b). Agarose has excellent optical transparency, film-forming ability, high mechanical strength (Z. Wang et al., 2010 b) and most interestingly it follows sol-gel transition at *ca.* 42$^{o}$C (Medina-Esquivel, Freile-Pelegrin, Quintana-Owen, Yáñez-Limón, & Alvarado-Gil, 2008) which could potentially prevent nanoparticle precipitation, agglomeration and thus maintaining good dispersion.

CNWs have been effectively incorporated into numerous biodegradable polymers e.g. poly lactic acid (PLA) (Hossain et al., 2012), poly caprolactone (PCL) (Boujemaoui et al., 2017), polyvinyl acid (PVA) (W. J. Lee, Clancy, Kontturi, Bismarck, & Shaffer, 2016), chitosan (Celebi & Kurt, 2015) and agar (Atef, Rezaei, & Behrooz, 2014), revealing a significant enhancement in mechanical and physical properties of their nanocomposites. Water soluble natural biopolymers reinforced with CNWs have been explored for wound dressing and drug coating and delivery applications (Zakir Hossain et al., 2012).

Highly transparent agarose films containing polyoxometalates were investigated as photochromic materials for high-density memory devices and portable high-resolution

display applications (Z. Wang et al., 2010 b). Xiaodong *et al*. investigated the mechanical properties of agarose nanocomposite films containing varying weight fractions of nanoclay, up to 80% (Xiaodong et al., 2005). Good agreement was observed for elastic moduli obtained from tensile and flexural tests. The elastic modulus of the nanoclay reinforced agarose increased gradually to 21.4 GPa, six times higher than plain agarose alone, with 60 wt% of nanoclay concentration, whereas ductility (failure strain) for the composites decreased from 0.24 to 0.02 as the concentration of nanoclay increased to 40 wt% (Xiaodong et al., 2005).

The influence of incorporating dried CNWs on the mechanical and physical properties of agar was explored (Atef et al., 2014; Oun & Rhim, 2015). Tensile strength and modulus of the agar films increased by 25% and 40% by inclusion of 5wt% of CNWs, whilst the optical transmittance decreased by ca. 18%. Both studies concluded that 5 wt% of CNWs was the highest content to enhance or even maintain the mechanical properties of agar films.

In this study, highly transparent nanocomposite films based on agarose and never-dried (i.e. in aqueous suspension) CNWs (used as reinforcement) were prepared using solution casting/evaporation method at higher concentrations of CNWs (0, 16, 28 and 43 wt%). The influence of CNWs inclusion on the morphological, surface roughness, light transparency, crystallisation, mechanical, thermo-mechanical and swelling kinetic properties of Agarose/CNWs blended films were investigated.

## Materials and methodology

### Materials

DNA Grade agarose powder (Electran®, Mw 120,000 Da, gelling temperature 34-37°C and melting point 60-90°C) was obtained from VWR international Ltd, UK. Sulphuric acid (95% purity), amberlite MB 6113 resin and bleached cotton wool were purchased from Fisher Scientific (UK).

### Preparation of cellulose nanowhiskers (CNWs)

The CNWs were produced by acid hydrolysis of cotton using aqueous sulfuric acid (64 wt%) for 45 min under continuous stirring (Hossain et al., 2012; Hossain et al., 2014). The residual acid was then removed from the hydrolysed CNWs suspension via centrifugation (three cycles at 10,000 rpm at 10°C for 20 min using de-ionised water) and dialysis under running tap water for 48 h. The CNWs/water suspension was then dispersed utilising a Branson sonicator

followed by filtration using a grade No. 2 fritted glass filter. The CNWs suspension was treated overnight with Amberlite resin to obtain $H_3O^+$ cation free CNWs suspension. The final concentration of CNWs in the de-ionised water was determined to be 1.15 wt%. This kind of as-prepared aqueous suspended CNWs was identified as never-dried CNWs (Agarwal, Ralph, Reiner, & Baez, 2016; K.-Y. Lee & Bismarck, 2012). On the other hand, dried crystalline CNWs were also produced via a freeze-drying process after freezing in liquid nitrogen as described elsewhere (Labet & Thielemans, 2011).

**Preparation of aqueous CNWs reinforced agarose films**

The aqueous cellulose nanowhisker reinforced agarose films (Agarose-CNW) were prepared by solution casting followed by film drying process, see Figure 1. The aqueous CNWs suspension in de-ionised water (1.15 wt%) was sonicated for 5 min. Afterwards, different quantities of the CNWs suspension (0, 5, 10 and 20 ml) were diluted with de-ionised water to reach 50 ml and then a fixed amount of Agarose powder (0.3 g) was added. The mixture was subjected to heat at 100°C with vigorous stirring using a hot plate magnetic stirrer and boiled for 5 min until the agarose powder had fully dissolved and the solution became clear with no obvious signs of sedimentation. The solution was then poured into a polystyrene petri-dish. The Agarose-CNWs solution was converted into gel within 5 min as the temperature dropped below 40°C. The nanocomposite hydrogels were allowed to dry at room temperature for 48 h to obtain flexible nanocomposite films of approximately 60 µm thickness. The nanocomposite films produced were further dried in a vacuum oven at 50°C for 48 h to eliminate any moisture traces present prior to testing.

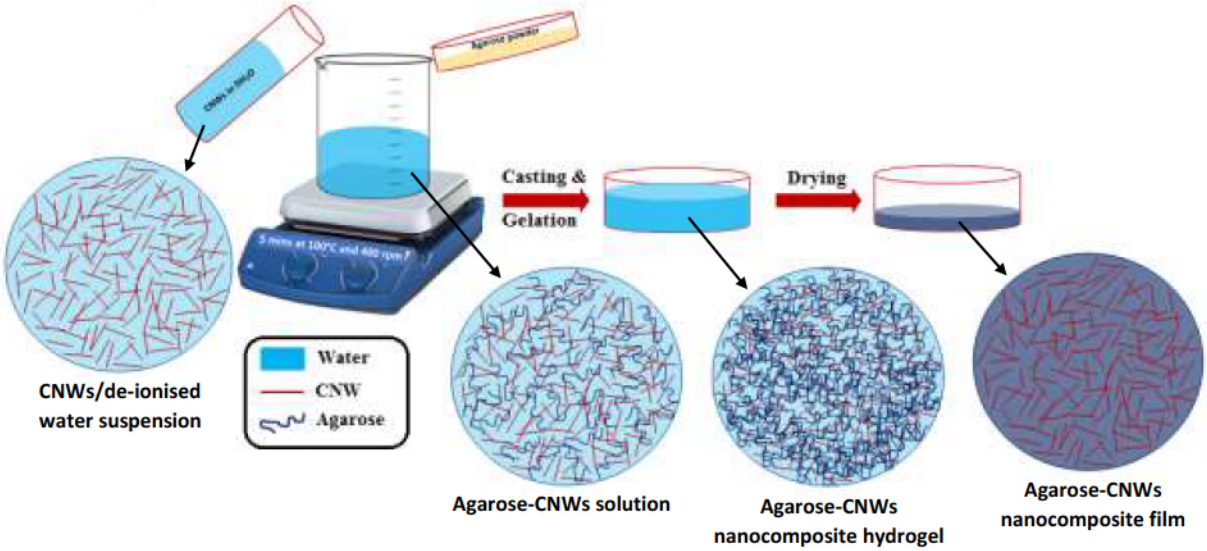


**Figure 1:** *A schematic diagram of the preparation process of Agarose-CNW nanocomposites films. In the solution state, CNWs and agarose chains were homogenously dispersed within the deionised water via stirring at 100°C. After casting the nanocomposite mixture and temperature dropped below 42°C, the agarose was converted into gel and thus maintained the uniform distribution of non-agglomerated CNWs with the agarose matrix. Water was then removed by drying at room temperature.*

Final concentration of the CNWs (wt%) within various Agarose-CNW nanocomposites was then calculated and have been tabulated (please see Table 1). The number used for the sample codes was considered according to the calculated weight fraction of CNWs within the nanocomposites.

**Table 1:** Sample codes and formulations of films prepared using never-dried CNWs and Agarose.

| Sample **codes** used in this study | Agarose (g) | De-ionised water (ml) | Never-dried CNWs suspension* (ml) | CNWs (wt%) |
|---|---|---|---|---|
| Agarose | 0.3 | 50 | 0 | 0 |
| Agarose-16 CNW | 0.3 | 45 | 5 | 16 |
| Agarose-28 CNW | 0.3 | 40 | 10 | 28 |

| | | | | |
|---|---|---|---|---|
| Agarose-43 CNW | 0.3 | 30 | 20 | 43 |

*Concentration of CNWs in de-ionised water 1.15%

**Characterisation**

**Electron microscopic analysis**

The surface morphology of freeze-dried CNWs was examined using scanning electron microscopy (SEM - Philips XL30, FEI, USA) at an accelerating voltage of 12 kV and a working distance of 10 mm. A sputtered platinum coating was employed to avoid image distortion due to charging.

The morphology of the never-dried CNWs was characterised using transmission electron microscopy (TEM, JEOL, 2000FXII, UK) at an accelerating voltage of 80 kV. The never-dried CNWs sample loaded on Cu-grid (mesh size 300) was stained negatively with 2 wt% uranyl acetate (Sigma-Aldrich, UK) to enhance the contrast.

**Atomic force microscopy (AFM) analysis**

AFM micrographs and roughness measurements of Agarose-CNW nanocomposite films were performed in tapping mode utilising a Bruker Dimension Icon equipped with AFM tips (model RTESPA-150 0.01–0.025 Ohm-cm Antinomy (n) doped Si). All measurements were carried out over a scan area of 2 and 5 $\mu m^2$. The micrographs obtained were analysed using Nanoscope analysis software (Version 1.5) and roughness analysis ($R_a$) was determined from at least three scans.

**Light Transmittance**

Light transparency property of the Agarose-CNW nanocomposite films was determined by measuring the light transmittance using a UV-Vis spectrometer (PerkinElmer, Lambda-25) over the wavelength range of 200 to 800 nm.

**Polarised light microscopy and image analysis**

Polarised optical microscope (Nikon Eclipse LV100ND, Nikon Instruments, Japan) equipped with a Nikon digital sight DS-Ri1 camera and a NIS Elements software (version 4.1) was used to examine the crystalline morphology of Agarose-CNW nanocomposites films. A small piece of film was placed on a microscope glass slide and the images were captured in transmission

mode between crossed polarisers at 20x optical magnification. A fixed intensity of incident light and an exposure time of 60s were used for all specimens.

**X-ray diffraction (XRD) analysis**

X-ray diffraction patterns for Agarose-CNW nanocomposites were determined using a D500 diffractometer (SIEMENS) equipped with a Cu-Kα radiation source (λ= 0.154 nm) at 15 mA and 30 kV. The samples were scanned from 5° to 45° diffraction angle (2θ) with step size of 0.05° and 2 s time interval.

The crystallinity index (CI%) of the films was calculated according to Equation 1 (Segal S., 1959; Weimer, Hackney, & French, 1995; Xu et al., 2013):

$$CI\ [\%] = \frac{I_{(Crys+am)} - I_{(am)}}{I_{(Crys+am)}} \times 100 \ldots\ldots\ldots\ldots\ldots\ldots (1)$$

where, $I_{(Crys+am)}$ denotes the most intense peak attributed to the combined crystalline and amorphous parts of cellulose (peak intensity at 2θ=22.8°), whereas $I_{(am)}$ represents the amorphous portion of cellulose (peak intensity usually appeared at 2θ=18°).

**Fourier transform infrared spectroscopy (FTIR)**

The functional groups present in CNWs, pure Agarose and their nanocomposite films were identified using a FTIR spectrometer (Tensor-27, Bruker, Germany) equipped with a standard attenuated total reflectance (ATR) cell (Pike Technology, UK). The films were scanned in transmittance mode over the wavenumber range from 4000 to 550 $cm^{-1}$ and the spectra were analysed using OPUS™ software (version 5.5).

**Tensile properties**

Tensile properties of Agarose-CNW films were determined using an Instron tensile testing machine attached with a 100 N load cell at speed of 1 mm $min^{-1}$ and 25 mm gauge length according to standard BS EN ISO 527-1:2012. Rectangular test specimens with a dimension of 55 mm length and 5 mm width were used. Tensile strength and modulus were calculated according to standard BS EN ISO 527-1:2012. At least 5 replicates of each film were tested.

**Dynamic mechanical analysis (DMA)**

Thermo-mechanical properties of the Agarose-CNW films were measured using a DMA tester (TA Q800 Instruments, USA) in multi-frequency strain mode to investigate the storage modulus (*E'*) and tan delta of the flexible films with increasing temperature. Rectangular test specimens (25 mm length and 4 mm width) were heated from room temperature to 280°C at a heating rate of 10°C $min^{-1}$, 0.05% strain, 15 mm gap distance, 0.01N preload force, 1 Hz frequency and 125% force track.

**Swelling kinetics**

The swelling capacity of the pure Agarose and Agarose-CNW nanocomposite films (10 mm disc) were calculated gravimetrically by measuring the variation in mass of the sample after soaking in phosphate buffered saline (PBS) media (10 ml) at 37°C for 24 h using Equation 2. At each time point, the wet samples were taken out from the media and placed onto tissue paper, blot dried and weighed immediately.

$$Swelling\,capacity\,(\%) = \frac{(M_w - M_i)}{M_i} \times 100 \quad \text{.....(2)}$$

where, $M_i$ is the initial mass of the dry specimen before immersion in PBS media and $M_w$ is the mass of wet specimen at each time point after soaking in PBS media.

## Results and Discussion

### Morphology and surface topography of CNWs

The morphology and surface topography of freeze-dried CNWs were characterised using SEM and AFM micrographs. The freeze-dried CNWs exhibited flake-like morphology at micron-range size due to the aggregation nature of CNWs (Khoshkava & Kamal, 2014) as seen in Figure 2a. The 2D AFM images (height) of the freeze-dried CNWs presented in Figures 2b also revealed aggregated morphology with a surface roughness value of 75 ± 7 nm from the 3D AFM image (see Figure 2c). On the other hand, TEM image of the aqueous CNWs suspension produced is presented in Figure 2d which revealed rod-like particles with average length and width approximately 300 ± 100 nm and 10 ± 2 nm, reported previously (Hossain et al., 2012). Individual rod-like morphology with the percolated network was also seen via the 2D AFM image of aqueous CNWs (see Figure 2e) and their surface roughness was found to be 11 ± 3 nm obtained from the 3D AFM image presented in Figure 2f.

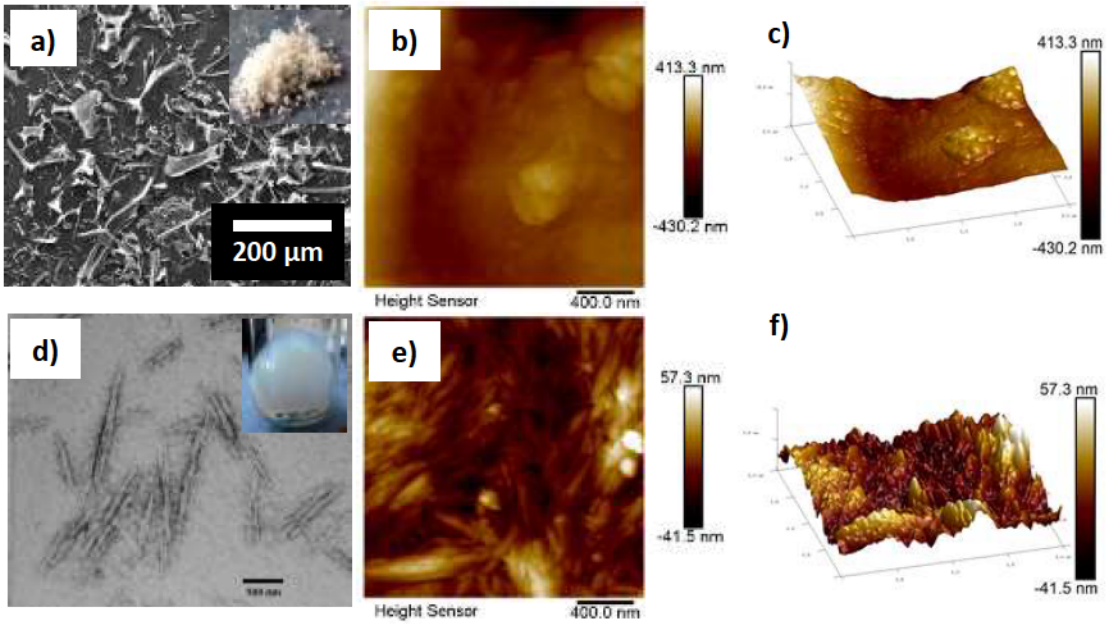


***Figure 2:*** *Morphology and surface topography of freeze-dried and never-dried CNWs:* ***a)*** *SEM image of freeze-dried CNWs (inset photograph of freeze-dried CNWs),* ***b-c)*** *AFM images of freeze-dried CNWs, 2D (b) and 3D (c),* ***d)*** *TEM image of never dried CNWs (inset photograph of never-dried CNWs suspension in deionised water, 1.15 wt%), and* ***e-f)*** *AFM images of never-dried CNWs, 2D (e) and 3D (f).*

Pure cellulose nanowhisker films were also produced from both freeze-dried and never-dried CNWs suspension (1.15 wt% in deionised water) via drying process at room temperature to observe their optical transparency. The freeze-dried CNWs film appeared to be white with a paper-like opaque appearance (see the supplementary figure, ESI 1a). This was in well agreement with the aggregated morphology and comparatively higher surface roughness (75 ± 7 nm) of the freeze-dried CNWs obtained via SEM and AFM images (as presented in Figures 2a-c). Alternatively, the aqueous CNWs prepared film presented in the supplementary figure (ESI 1b) was observed to be translucent which was suggested to be due to their well dispersed rod-like CNW structures as well as their comparatively lower surface roughness (11 ± 3 nm). However, both films obtained from freeze-dried and aqueous CNWs were brittle and cracked during the drying stage as seen in the supplementary figure (ESI 1).

**Light transparency**

Considering the suggested better dispersion and superior light transparency properties of the aqueous CNWs over the freeze-dried CNWs films (Atef et al., 2014), then various contents of aqueous CNWs were blended with Agarose to investigate the production of flexible and

transparent nanocomposite films. Agarose-CNW nanocomposite films were prepared by solution casting/evaporation process by mixing never-dried CNWs suspension with agarose powder at high temperature (100°C) until agarose powder fully dissolved and followed by casting and drying at room temperature, see Figure 1. Agarose is a thermo-responsive hydrogel that could convert quickly from solution state to a gel state as the temperature dropped below *ca.* 42°C (Medina-Esquivel et al., 2008). This property could potentially prevent nanoparticle precipitation and agglomeration during the drying step of the nanocomposite films. Representative images of the flexible films (see Figures 3a-d) revealed that the optical transparency decreased with increasing CNWs content (as expected). The light transparency of the nanocomposite films obtained by UV/Visible spectrometry also showed that the pure Agarose film exhibited light transparency of 91% in most of the visible light region (at 650 nm wavelength), whereas, the Agarose-CNW nanocomposites exhibited decreasing light transmittance with values of 90, 89 and 84% with increasing CNWs content (ranging from 16, 28 and 43 wt%). The optical transparency of agar film was reported to decrease more than 30% by inclusion of 10 wt% freeze-dried CNWs as a result of their agglomeration (Atef et al., 2014). Reduction in the optical transparency by increasing the nanoparticles content has been also reported for other highly transparent polymer nanocomposites (Dang et al., 2014; C. Liu et al., 2017).

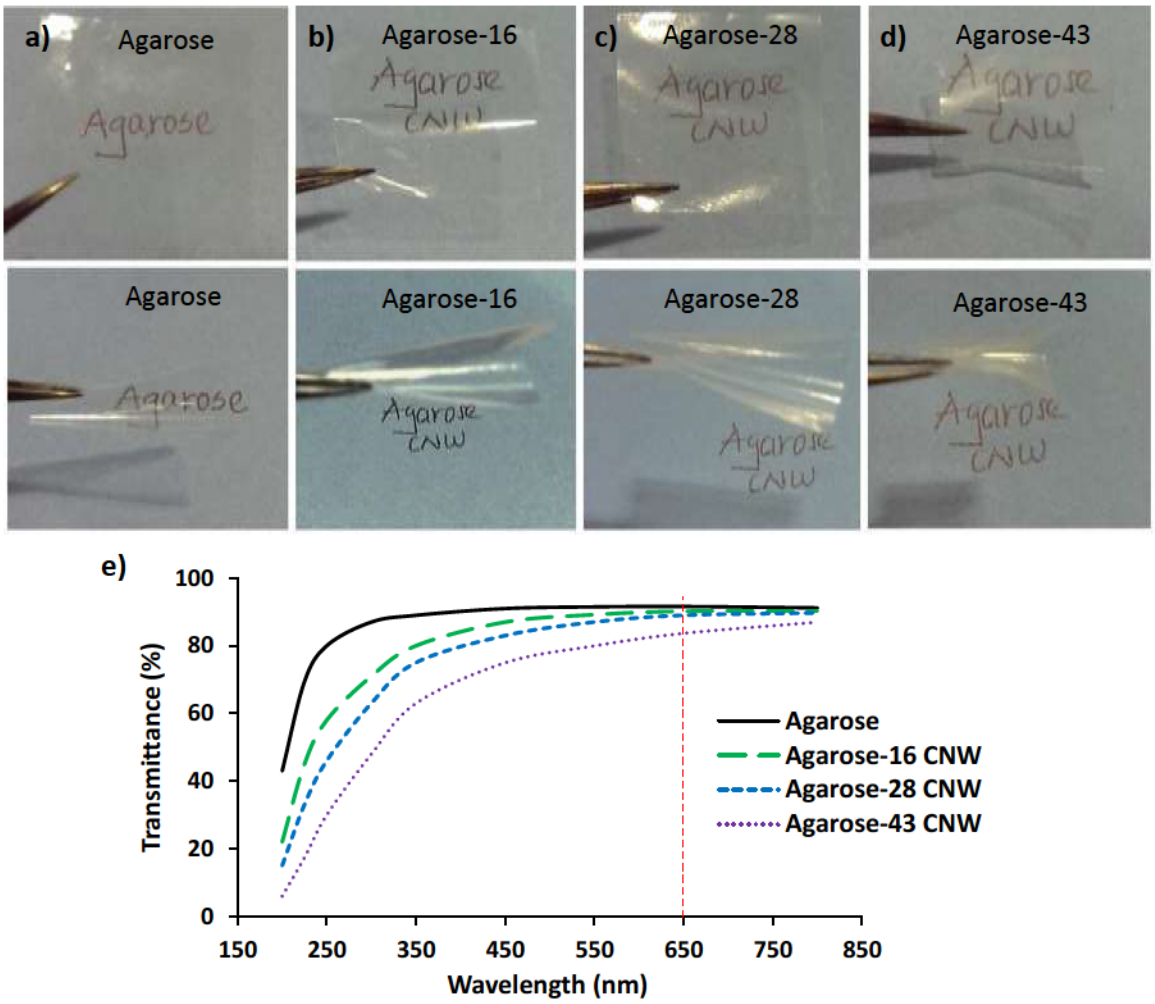


***Figure 3:*** *Representative photographs of the transparent (top) and flexible (bottom) thin films:* ***a)*** *Agarose,* ***b)*** *Agarose-16 CNW,* ***c)*** *Agarose-28 CNW and* ***d)*** *Agarose-43 CNW. e) Light transmittance of flexible thin films obtained by UV/Visible spectrometry.*

**Surface roughness and polarised light micrographs**

The surface topography of the Agarose-CNW films was also characterised by AFM analysis and the 3D AFM surface topography images are presented in Figures 4a-d. The surface roughness (Ra) of the pure Agarose film was found to be 8 ± 2 nm, whereas, the nanocomposites exhibited surface roughness of 7 ± 2 , 7 ± 2 and 15 ± 3 nm for Agarose-16 CNW, Agarose-28 CNW and Agarose-43 CNW films, respectively. The addition of up to 28 wt% aqueous CNWs within the nanocomposite films showed no significant change in their surface roughness, which correlated with the optical transparency properties (89-91% transmittance at 650 nm wavelength). However, a significant increase in surface roughness 15 ±3 nm was found for the film containing 43 wt% aqueous CNWs suspension. This was attributed to the

presence of higher amount of CNWs which tend to aggregate in the nanocomposites resulting in a decrease in their light transparency to 84%. Nogi *et al.* also reported that the rough surface of the nanocellulose film significantly reduced the light transmittance property due to light scattering effect (Nogi, Iwamoto, Nakagaito, & Yano, 2009). Further 2D AFM images showing surface topography of the nanocomposite films produced can be seen in the supplementary figure (ESI 2).

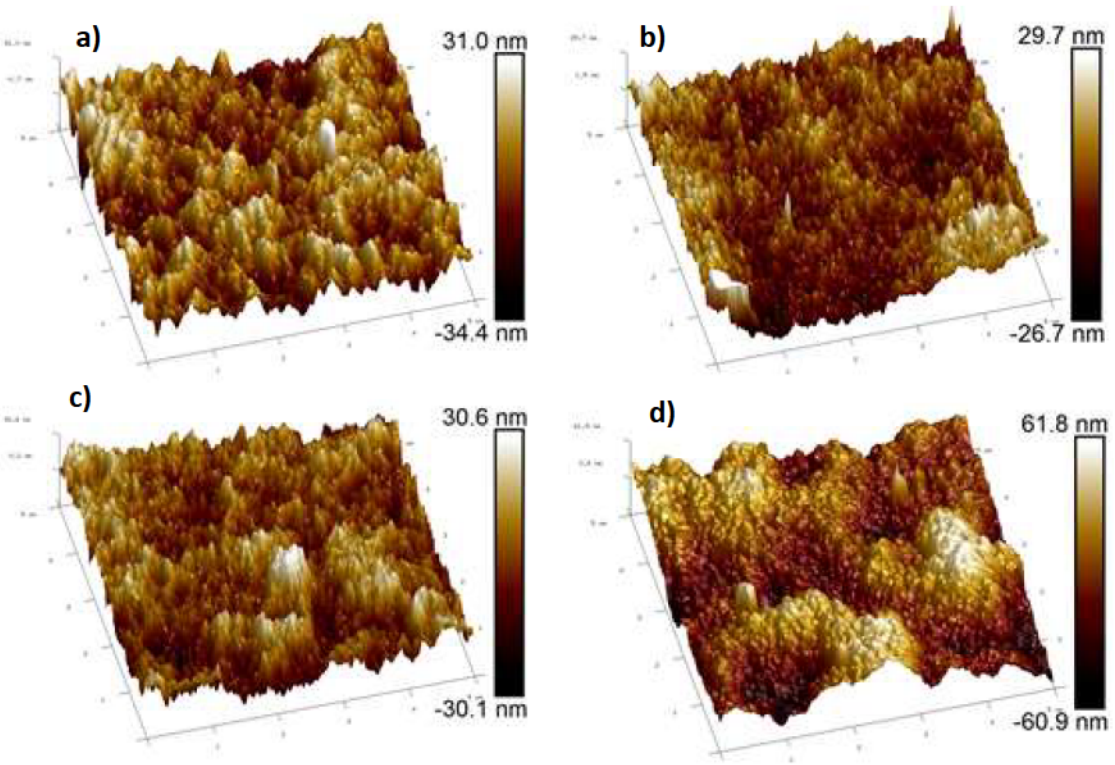


***Figure 4:*** *3D AFM images showing the surface topography of the thin films:* ***a)*** *Agarose,* ***b)*** *Agarose-16 CNW,* ***c)*** *Agarose-28 CNW and* ***d)*** *Agarose-43 CNW.*

Polarised light micrographs revealed clear morphological differences between the pure Agarose and nanocomposite films containing varying quantities of CNWs (see Figure 5). A blank image of the crossed polarisers (completely black, seen in Figure 5a was also carried out without any samples present. Absent of any white dots or bright field in the control Agarose film (see Figure 5b) indicated absence of any crystalline domains within the matrix. The nanocomposite films (see Figures 5c-e) revealed distribution of bright areas with a number of white dots within the films which was attributed to the birefringence arising from crystalline domains of the CNWs (Chowdhury, Peng, & Youngblood, 2017). An increase in the brightness for the nanocomposite films indicated that the dispersion of CNWs increased with an increase

in their content within the agarose matrix. However, an increasing number of white dots within the higher CNW-content films were observed. These were suggested to be due to the self-association nature of CNWs and the high CNW content within the composites (Parker et al., 2016). These limited aggregations in the nanocomposites was expected with increasing cellulose content and correlated well with the surface roughness and optical transparency properties of the nanocomposite films obtained. A similar aggregated morphology was also reported for high CNWs content (up to 75 wt%) flexible films prepared using CNWs and hydroxyethyl cellulose (Zakir Hossain et al., 2012). Aqueous CNWs films also showed a pattern of bright field and distribution of white dots (as presented in Figure 5f) due to their homogeneous dispersion and a percolated network of these larger domains (Xu et al., 2013).

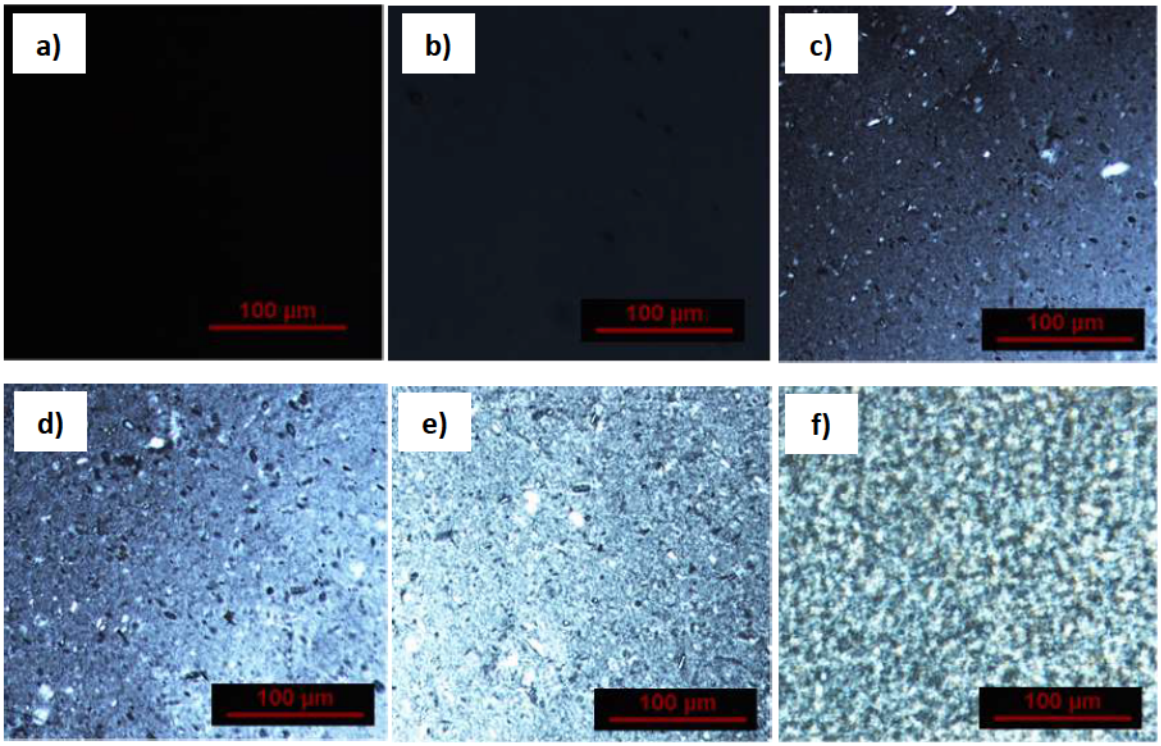


***Figure 5:*** *Cross-polarised optical microscope images of the nanocomposite films:* ***a)*** *blank (no film),* ***b)*** *Agarose,* ***c)*** *Agarose-16 CNW,* ***d)*** *Agarose-28 CNW,* ***e)*** *Agarose-43 CNW and* ***f)*** *CNWs film.*

**Crystallisation properties**

XRD patterns of the CNWs, pure Agarose and Agarose-CNW flexible films are presented in Figure 6a. The diffraction pattern of CNWs demonstrated the characteristic intense peak at 22.8°, with an additional double peak signal at 14.9° and 16.5° which was consistent with the diffraction pattern of cellulose (reference ICDD PDF-2 database, File no. 00-050-2241) (Abou-

Sekkina, 1986). The CNWs were calculated to contain 89.1% crystallinity, which was also similar to the results stated in other studies (~88.6%) (Heath & Thielemans, 2010). The pure Agarose films showed a halo◊ typical diffraction pattern of amorphous materials at 2θ = 19° and all nanocomposite films exhibited a clear retention of the cellulose crystallites with increasing peak intensity at diffraction angles around 14.9 °, 16.5° and 22.8°. The overall crystallinity of the nanocomposite films was seen to increase (up to 79% for Agarose-43 CNWs film) with the addition of CNWs into the Agarose matrix (see Figure 6b), which suggested that the CNWs acted as nucleating agents within the Agarose matrix via the alignment of agarose chain structure along the CNWs surfaces due to hydrogen bonding (D. Y. Liu, Yuan, Bhattacharyya, & Easteal, 2010; Zakir Hossain et al., 2012). The increase in crystallinity of the nanocomposites films could also be responsible for the slight reduction in their optical transparency (S. G. Lee et al., 2009), see Figure 3e.

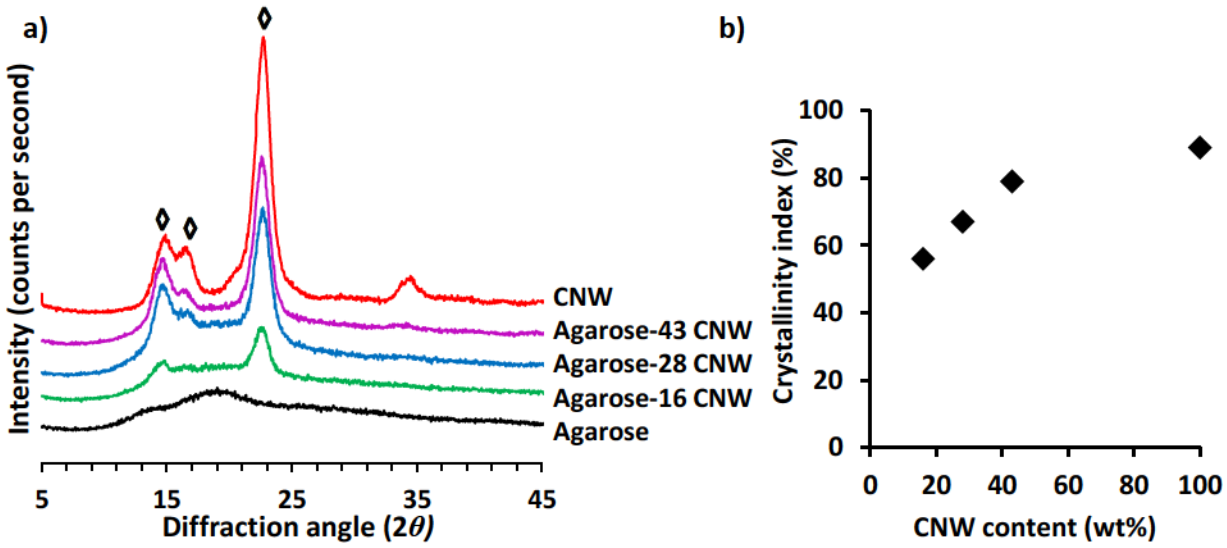


***Figure 6: a)*** *XRD Diffraction pattern of pure CNWs, control Agarose and nanocomposite films produced using various blends of Agarose and CNWs. ◊ = Reference cotton-based cellulose peaks identified from the ICDD patent PDF-2 database (File no. 00-050-2241), and* ***b)*** *relationship between the crystallinity index (CI) and CNWs content in the flexible films.*

**FTIR analysis**

The functional groups of the CNWs, pure Agarose and the nanocomposite films were identified using FTIR-ATR analysis as presented in Figure 7a. The pure Agarose film exhibited a characteristic broad band around 3100-3550 $cm^{-1}$ with highest peak at 3363 $cm^{-1}$ which was attributed to –OH stretching vibration. Pure CNWs also showed a similar broad spectrum peak

at 3336 $cm^{-1}$ was attributed to free –OH stretching vibration (Trivedi, Rao, & Kumar, 2014). In case of the Agarose-CNW nanocomposites, peaks associated with the -OH stretching vibration were also observed at 3336 $cm^{-1}$ (-OH stretching vibration peak of the CNWs), which was suggested to be due to the formation of hydrogen bonds between -OH groups of CNWs and agarose as indicated in Figure 7b. Similar types of hydrogen bonding were also reported for agarose-chitosan blends (Trivedi et al., 2014). The bands at 2900 $cm^{-1}$ and 1429 $cm^{-1}$ indicated the C-H stretching (for both agarose and CNWs) and bending of $–CH_2$ (agarose only) groups, respectively. The peak at 1162$cm^{-1}$ was attributed to the C-O-C stretching bridge of glucose ring structure of cellulose. The bands at 1057 $cm^{-1}$ and 1032$cm^{-1}$ represented the C-O stretching at position C-6 and C-3 in the saccharide structure, respectively (Q. Li, Zhou, & Zhang, 2009). Agarose-CNW nanocomposites also showed the characteristics absorbance bands of agarose at 931 $cm^{-1}$ (due to 3,6-anhydrogalactose bending), 1151 and 1040 $cm^{-1}$ (attributed to C—O stretching vibration) (Chaudhary, Vadodariya, Nataraj, & Meena, 2015) and 1635 $cm^{-1}$ (due to the C=O stretching vibration) (Trivedi et al., 2014).

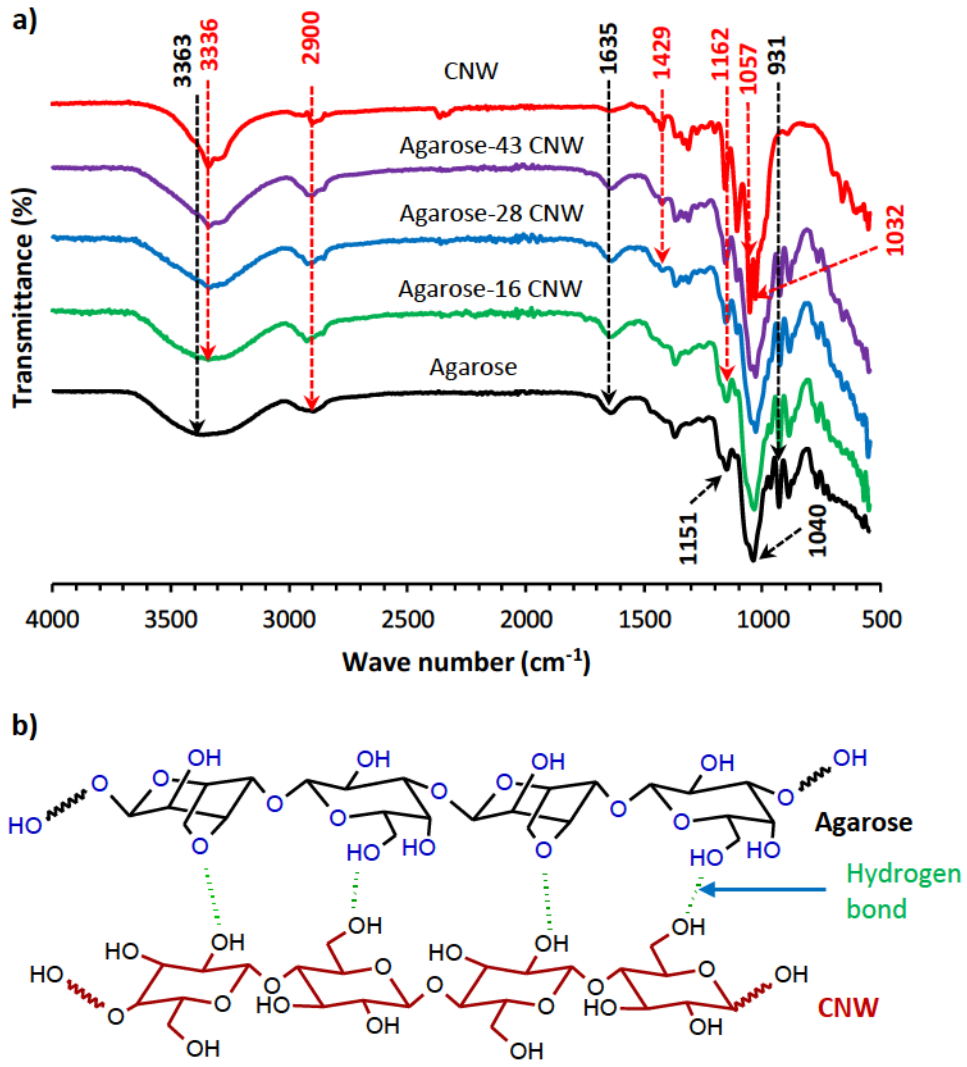


***Figure 7: a)*** *FTIR spectra of pure CNWs, control Agarose and nanocomposite films produced using various blends of Agarose and CNWs, and* ***b)*** *schematic illustration for the expected chemical interaction between agarose and CNWs within the nanocomposite films (green dot lines represent the hydrogen bonding).*

**Mechanical properties**

The tensile properties of the nanocomposite films are shown in Figure 8a, where all the Agarose-CNW nanocomposite films displayed an increase in tensile strength and modulus properties when compared to the pure Agarose film. For example, *ca*. 30% and 90% increase in tensile strength and modulus was observed for Agarose-16 CNW compared to pure Agarose film (tensile strength 46 ± 2 MPa and modulus 1.7 ± 0.1 GPa). An increase in tensile properties was expected due to the reinforcing effect of the CNW nanofillers (longitudinal tensile modulus of cotton based CNWs 57-105 GPa (Rusli & Eichhorn, 2008)). However, no significant

change was seen in tensile strength (*ca.* 90 MPa) of the nanocomposites films as the CNWs increased from 16 to 42 wt%. Moreover, the difference in the tensile modulus between Agarose-43 CNW film (4.2 ± 0.1 GPa) compared to Agarose-28 CNW film (4.1 ± 0.3 GPa) was insignificant. This was suggested to be due to the tendency of CNWs to agglomerate (Xu et al., 2013) within the matrix (at higher CNWs loading content) which was in a good agreement with observations from the polarised light microscopy images.

From the stress-strain curves (see Figure 8b), a decrease in strain at break was seen with the addition of CNWs for all Agarose-CNW nanocomposites in comparison with the pure Agarose film, suggesting the addition of CNWs made the Agarose-CNW nanocomposite films relatively rigid (Shumigin, Tarasova, Krumme, & Meier, 2011), which was expected for nanocomposite materials (Moon, Martini, Nairn, Simonsen, & Youngblood, 2011).

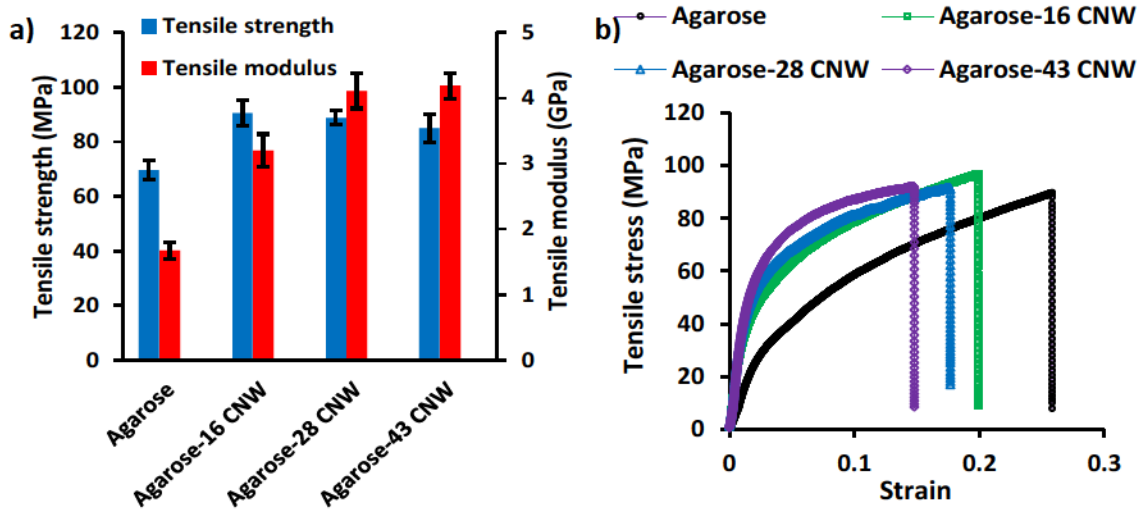


***Figure 8: a)*** *Tensile strength and modulus curves and b) representative stress-strain curves of control Agarose and various Agarose-CNW nanocomposite films. Five replicates (n=5) of each specimen were tested and the mean (±SD) is presented.*

**Thermo-mechanical properties**

DMA was used to obtain the storage modulus of the nanocomposite films as a function of temperature (Figure 9a). The DMA test showed that the Agarose-CNW nanocomposite films demonstrated good stability against temperature up to and beyond 200°C as shown in Figure 9. The addition of CNWs within the Agarose matrix showed a significant increase in storage modulus properties for all compositions with increasing CNWs content over the whole temperature range investigated (25 to 280°C). The storage modulus of the nanocomposite

films increased to reach *ca.* 300% of Agarose alone as the CNWs content increased to 43 wt%. Nanofillers blended with polymer was also reported to improve the storage modulus of the matrix at higher temperatures due to their higher interfacial surface area, and surface induced crystallisation within the nanocomposites (Petersson, Kvien, & Oksman, 2007; Zakir Hossain et al., 2012).

Tan delta curves of the Agarose-CNW flexible films are presented in Figure 9b. Agarose-16 CNW film revealed that the tan delta peaks had shifted slightly to a higher temperature region (268°C) as compared to pure Agarose film (263°C), which indicated that the incorporated CNWs governed the reduction in the segmental motions of the Agarose matrix in the blends through CNW-Agarose interactions (Petersson et al., 2007). However, 28 and 43 wt% addition of CNWs within the nanocomposite films resulted in a shift of tan delta peaks to lower temperature region (257°C and 212°C, respectively). This was suggested to be due to the thermal degradation of cotton based acid hydrolysed CNWs which was reported to be initiated at around 200°C with major decomposition at 261°C (Zakir Hossain et al., 2012). At higher nanofiller loading it was anticipated that the presence of a considerable amount of aggregated CNWs (as confirmed earlier by the white dots obtained via polarised light microscopy images) was believed to be loosely bound within the matrix. These poorly bound aggregated CNWs were expected to degrade after 200°C as they are not firmly protected by the matrix thus leading to heat induced failure of the nanocomposite films, which was also obvious from the tan delta curve (film broke at ~212°C) of the Agarose-43 CNW film.

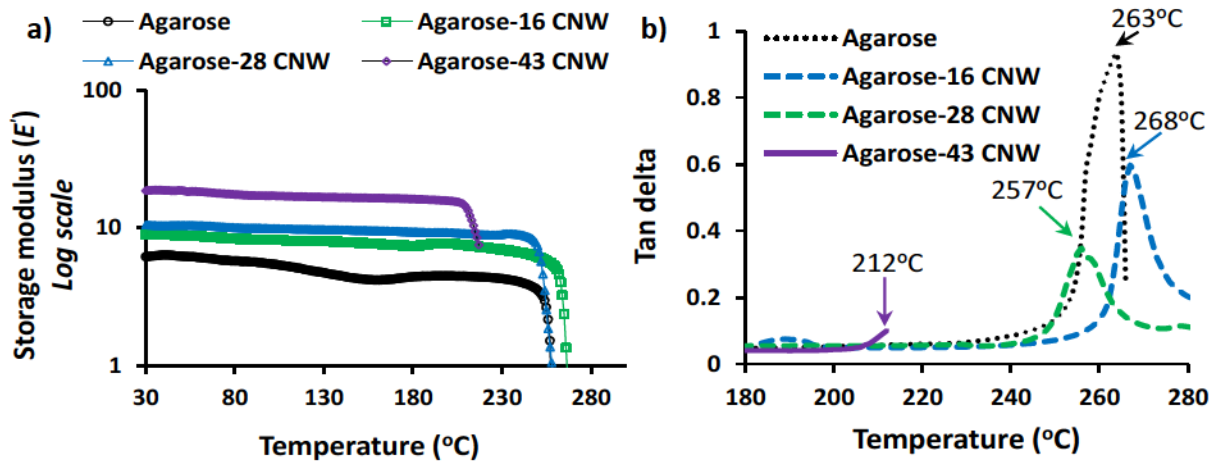


***Figure 9:*** *a) storage modulus curves and b) tan delta curves of thin films produced using various composites of Agarose and CNWs. Five replicates (n=5) of each specimen were tested and the mean (±SD) is presented.*

**Swelling kinetics**

The swelling capacity, i.e. percentage of weight change due to water absorption, of control Agarose and Agarose-CNW nanocomposite films in PBS media at 37°C with swelling time is presented in Figure 10a. The incorporation of CNWs within the matrix led to a significant decrease in the swelling capacity of the nanocomposites suggesting the presence of a greater degree of CNW-CNW interaction which was believed to decrease the hydrophilicity by reducing the water holding capacity (W. Wang, Wang, Kang, & Wang, 2011; Zakir Hossain et al., 2012).

A swelling kinetics model (Schott's second order) was also introduced (Equation 3) (Schott, 1992; Zakir Hossain et al., 2012) to evaluate the theoretical swelling capacity and initial swelling rate of the Agarose-CNW nanocomposite films (W. Wang et al., 2011).

$$\frac{t}{Q_t} = \frac{1}{k_{is}} + \frac{1}{Q_\infty} \times t \quad \text{.....(3)}$$

Here, $Q_t$ (g/g) denotes the swelling capacity of the films at time t (s), $Q_\infty$ (g/g) is the theoretical equilibrium swelling capacity and $K_{is}$ (g/g) is the initial swelling rate constant.

A plot of $t/Q_t$ against $t$ was drawn using the experimental swelling data of Agarose-CNW films (see Figure 10b) and the linear trend line obtained for these experimental values showed high regression coefficients (>0.99), which justified the use of Schott's second-order swelling kinetics model for these nanocomposite films in PBS media (W. Wang et al., 2011). The theoretical equilibrium swelling capacity ($Q_\infty$) and the initial swelling rate constant (C. Liu et al.) were calculated using the linear regression equation: $Y = a + bX$, (where, $Y=t/Q_t$, $a=1/K_{is}$, $b=1/Q_\infty$ *and* $X=t$) obtained from the linear lines and plotted against CNWs content in the nanocomposite films in Figure 10c. The calculated theoretical swelling kinetic parameters ($Q_\infty$ and $K_{is}$) of the nanocomposite films were found to decrease with addition of CNWs content which suggested that the incorporation of CNWs into the matrix played a significant influence on decreasing swelling rate of the Agarose-CNW nanocomposite films. The values of $Q_\infty$ and $K_{is}$ decreased by *ca.* 50% of their values (280 $g.g^{-1}$ and 0.6 $g.g^{-1}.s^{-1}$) as the amount of CNWs reached 43 wt%.

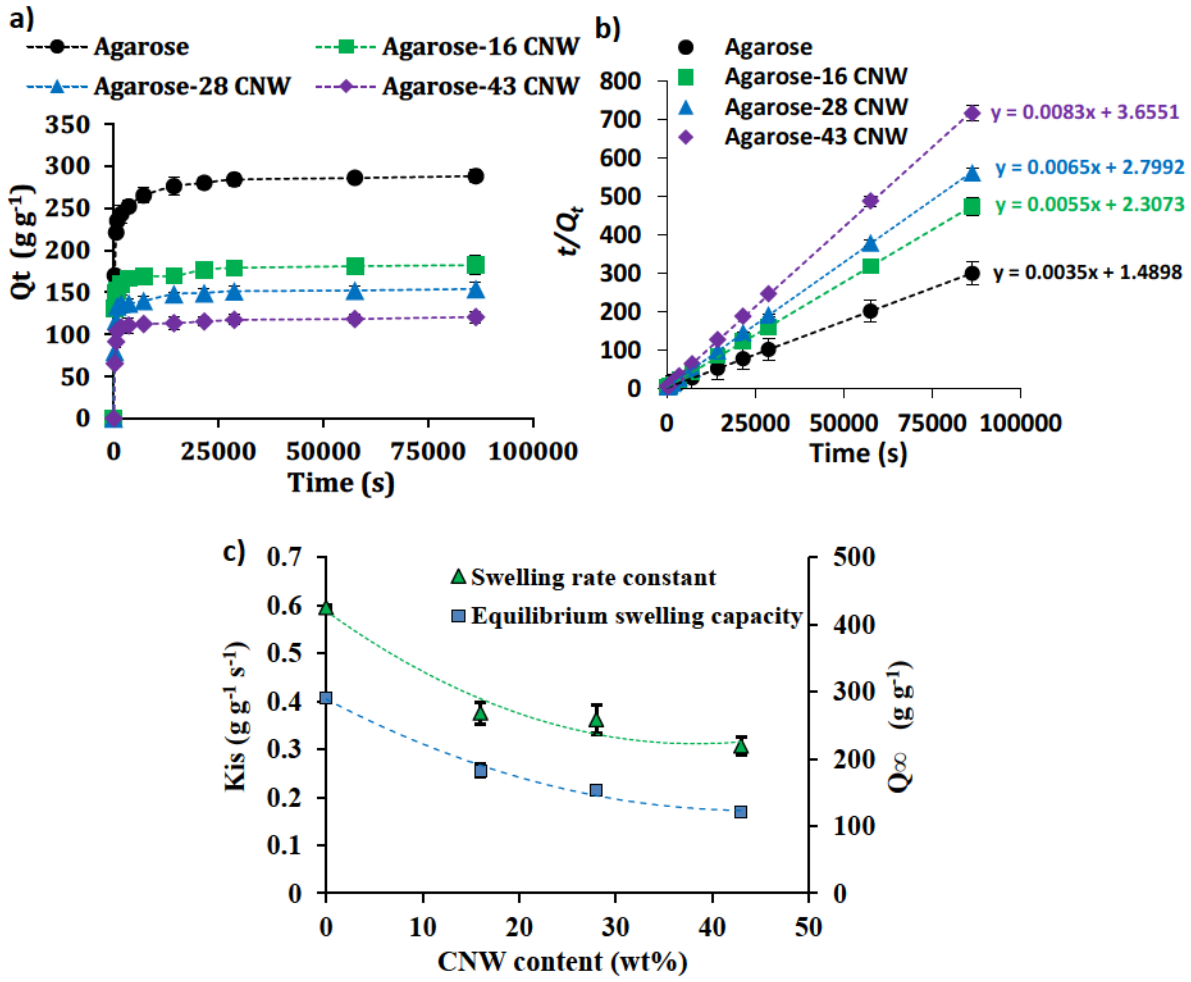


***Figure 10: a)*** *Swelling kinetic curves and b) Corresponding plots of $t/Q_t$ against t of the nanocomposite films produced using various blends of Agarose and CNWs. c) Relationship between the swelling rate constant and equilibrium swelling capacity with CNWs content in PBS media at 37°C. Five replicates (n=5) of each specimen were used in the swelling experiment and the mean (±SD) is presented.*

Most of the highly transparent polymer nanocomposites reported in the literature were obtained by in situ polymerisation technique and /or surface modification of the nanoparticles (Althues et al., 2007; Bin et al., 2011; Dang et al., 2014; C. Liu et al., 2017). In this study, a highly transparent Agarose-CNW nanocomposite was achieved, using conventional solution casting method and non-functionalised nanoparticles, benefiting from two characteristics of the nanocomposite constituents; sol-gel property of Agarose and suspension of the non-agglomerated CNWs. It was also found that incorporation of CNWs into the Agarose matrix provided significant increases in mechanical, thermomechanical and

crystallinity and decrease in the swelling capacity of the nanocomposites when compared to control Agarose films. These modified capabilities offer many potential applications for cellulose based composite films in tissue engineering, drug coating and encapsulation.

## Conclusions

This study presents a morphological, surface topographical and film forming properties of freeze-dried and aqueous suspended CNWs. The freeze-dried CNWs were seen to aggregate into flake-like geometries with higher surface roughness ($R_a$ ~75 nm) compared to the well dispersed needle-like aqueous CNWs ($R_a$ ~11 nm). Due to higher surface roughness the freeze-dried CNWs were found to form a white, opaque and brittle film, while the aqueous CNWs film was brittle and translucent. However, transparent and flexible films based on a range of Agarose-CNWs nanocomposite films were prepared in this study. Incorporation of never-dried CNWs within the matrix was seen to be well dispersed despite some limited aggregation within higher CNWs loaded film (43 wt%), which played an influential role on the surface roughness ($R_a$ below 15 nm for all nanocomposite films) and optical transparency properties of the nanocomposite films (transparency more than 84%). An increase in crystallinity of nanocomposite films with CNWs content suggested that the CNWs acted as nucleating sites to induce crystallisation within the Agarose matrix. The enhanced tensile strength, modulus and storage modulus properties of the nanocomposite films compared to the control Agarose film confirmed the reinforcing effect of the nanowhiskers The incorporation of CNWs also had a significant influence on controlling the swelling properties of Agarose-CNW blend films in aqueous media.

## References

Abou-Sekkina, M. M., Sakran, M.A. and Saafan, A.A. (1986). *Industrial & Engineering Chemistry Product Research and Development* 25, 676.

Agarwal, U. P., Ralph, S. A., Reiner, R. S., & Baez, C. (2016). Probing crystallinity of never-dried wood cellulose with Raman spectroscopy. *Cellulose,* 23(1), 125-144.

Althues, H., Simon, P., & Kaskel, S. (2007). Transparent and luminescent YVO4 : Eu/polymer nanocomposites prepared by in situ polymerization. *Journal of Materials Chemistry,* 17(8), 758-765.

Atef, M., Rezaei, M., & Behrooz, R. (2014). Preparation and characterization agar-based nanocomposite film reinforced by nanocrystalline cellulose. *International Journal of Biological Macromolecules,* 70(Supplement C), 537-544.

Aulin, C., Salazar-Alvarez, G., & Lindstrom, T. (2012). High strength, flexible and transparent nanofibrillated cellulose-nanoclay biohybrid films with tunable oxygen and water vapor permeability. *Nanoscale,* 4(20), 6622-6628.

Awadhiya, A., Tyeb, S., Rathore, K., & Verma, V. (2017). Agarose bioplastic-based drug delivery system for surgical and wound dressings. *Engineering in Life Sciences,* 17(2), 204-214.

Bin, C., Sugihara, O., Elim, H. I., Adschiri, T., & Kaino, T. (2011). An approach of high refractive index and highly transparent polymer nanocomposite fabrication. *17th Microopics Conference (MOC)* (pp. 1-2).

Boujemaoui, A., Cobo Sanchez, C., Engström, J., Bruce, C., Fogelström, L., Carlmark, A., & Malmström, E. (2017). Polycaprolactone Nanocomposites Reinforced with Cellulose Nanocrystals Surface-Modified via Covalent Grafting or Physisorption: A Comparative Study. *ACS Applied Materials & Interfaces,* 9(40), 35305-35318.

Camargo, P. H. C., Satyanarayana, K. G., & Wypych, F. (2009). Nanocomposites: synthesis, structure, properties and new application opportunities. *Materials Research,* 12, 1-39.

Cao, Z., Gilbert, R. J., & He, W. (2009). Simple Agarose–Chitosan Gel Composite System for Enhanced Neuronal Growth in Three Dimensions. *Biomacromolecules,* 10(10), 2954-2959.

Celebi, H., & Kurt, A. (2015). Effects of processing on the properties of chitosan/cellulose nanocrystal films. *Carbohydrate Polymers,* 133(Supplement C), 284-293.

Chaudhary, J. P., Vadodariya, N., Nataraj, S. K., & Meena, R. (2015). Chitosan-Based Aerogel Membrane for Robust Oil-in-Water Emulsion Separation. *ACS Applied Materials & Interfaces,* 7(44), 24957-24962.

Cheng, Y., Lu, C., Lin, Z., Liu, Y., Guan, C., Lu, H., & Yang, B. (2008). Preparation and properties of transparent bulk polymer nanocomposites with high nanophase contents. *Journal of Materials Chemistry,* 18(34), 4062-4068.

Chowdhury, R. A., Peng, S. X., & Youngblood, J. (2017). Improved order parameter (alignment) determination in cellulose nanocrystal (CNC) films by a simple optical birefringence method. *Cellulose,* 24(5), 1957-1970.

Cipiriano, B. H., Kashiwagi, T., Raghavan, S. R., Yang, Y., Grulke, E. A., Yamamoto, K., . . . Douglas, J. F. (2007). Effects of aspect ratio of MWNT on the flammability properties of polymer nanocomposites. *Polymer,* 48(20), 6086-6096.

Corthell, J. T. (2014). *Chapter 3 - Agarose Gel Electrophoresis*. In *Basic Molecular Protocols in Neuroscience: Tips, Tricks, and Pitfalls* (pp. 21-25). San Diego: Academic Press

Dang, A., Ojha, S., Hui, C. M., Mahoney, C., Matyjaszewski, K., & Bockstaller, M. R. (2014). High-Transparency Polymer Nanocomposites Enabled by Polymer-Graft Modification of Particle Fillers. *Langmuir,* 30(48), 14434-14442.

Ehlert, S., Stegelmeier, C., Pirner, D., & Förster, S. (2015). A General Route to Optically Transparent Highly Filled Polymer Nanocomposites. *Macromolecules,* 48(15), 5323-5327.

Gadjanski, I., Yodmuang, S., Spiller, K., Bhumiratana, S., & Vunjak-Novakovic, G. (2013). Supplementation of Exogenous Adenosine 5′ -Triphosphate Enhances Mechanical Properties of 3D Cell–Agarose Constructs for Cartilage Tissue Engineering. *Tissue Engineering Part A,* 19(19-20), 2188-2200.

George, J., & Sabapathi, S. N. (2015). Cellulose nanocrystals: synthesis, functional properties, and applications. *Nanotechnology, Science and Applications,* 8, 45-54.

Hassanabadi, H. M., & Rodrigue, D. (2014). Effect of Particle Size and Shape on the Reinforcing Efficiency of Nanoparticles in Polymer Nanocomposites. *Macromolecular Materials and Engineering,* 299(10), 1220-1231.

Heath, L., & Thielemans, W. (2010). Cellulose nanowhisker aerogels. *Green Chemistry,* 12(8), 1448-1453.

Hossain, K. M. Z., Ahmed, I., Parsons, A. J., Scotchford, C. A., Walker, G. S., Thielemans, W., & Rudd, C. D. (2012). Physico-chemical and mechanical properties of nanocomposites prepared using cellulose nanowhiskers and poly(lactic acid). *Journal of Materials Science,* 47(6), 2675-2686.

Hossain, K. M. Z., Hasan, M. S., Boyd, D., Rudd, C. D., Ahmed, I., & Thielemans, W. (2014). Effect of Cellulose Nanowhiskers on Surface Morphology, Mechanical Properties, and Cell Adhesion of Melt-Drawn Polylactic Acid Fibers. *Biomacromolecules,* 15(4), 1498-1506.

Iwamoto, S., Kai, W., Isogai, A., & Iwata, T. (2009). Elastic Modulus of Single Cellulose Microfibrils from Tunicate Measured by Atomic Force Microscopy. *Biomacromolecules,* 10(9), 2571-2576.

Jordan, J., Jacob, K. I., Tannenbaum, R., Sharaf, M. A., & Jasiuk, I. (2005). Experimental trends in polymer nanocomposites—a review. *Materials Science and Engineering: A,* 393(1), 1-11.

Kargarzadeh, H., Mariano, M., Huang, J., Lin, N., Ahmad, I., Dufresne, A., & Thomas, S. (2017). Recent developments on nanocellulose reinforced polymer nanocomposites: A review. *Polymer,* 132, 368-393.

Khalil, R., Homaeigohar, S., Häußler, D., & Elbahri, M. (2016). A shape tailored gold-conductive polymer nanocomposite as a transparent electrode with extraordinary insensitivity to volatile organic compounds (VOCs). *Scientific Reports,* 6, 33895.

Khoshkava, V., & Kamal, M. R. (2014). Effect of drying conditions on cellulose nanocrystal (CNC) agglomerate porosity and dispersibility in polymer nanocomposites. *Powder Technology,* 261(Supplement C), 288-298.

Labet, M., & Thielemans, W. (2011). Improving the reproducibility of chemical reactions on the surface of cellulose nanocrystals: ROP of ε-caprolactone as a case study. *Cellulose,* 18(3), 607-617.

Lee, K.-Y., & Bismarck, A. (2012). Susceptibility of never-dried and freeze-dried bacterial cellulose towards esterification with organic acid. *Cellulose,* 19(3), 891-900.

Lee, S. G., Lee, J. S., Ha, J.-W., Park, I. J., Lee, S.-B., & Lee, J. D. (2009). Effect of crystallinity on surface morphology and light transmittance of poly(vinylidene fluoride-co-hexafluoropropylene) thin film. *Journal of Applied Polymer Science,* 114(5), 3331-3337.

Lee, W. J., Clancy, A. J., Kontturi, E., Bismarck, A., & Shaffer, M. S. P. (2016). Strong and Stiff: High-Performance Cellulose Nanocrystal/Poly(vinyl alcohol) Composite Fibers. *ACS Applied Materials & Interfaces,* 8(46), 31500-31504.

Li, Q., Zhou, J., & Zhang, L. (2009). Structure and properties of the nanocomposite films of chitosan reinforced with cellulose whiskers. *Journal of Polymer Science Part B: Polymer Physics,* 47(11), 1069-1077.

Li, Y.-Q., Fu, S.-Y., Yang, Y., & Mai, Y.-W. (2008). Facile Synthesis of Highly Transparent Polymer Nanocomposites by Introduction of Core–Shell Structured Nanoparticles. *Chemistry of Materials,* 20(8), 2637-2643.

Liu, C., Li, Z., Hajagos, T. J., Kishpaugh, D., Chen, D. Y., & Pei, Q. (2017). Transparent Ultra-High-Loading Quantum Dot/Polymer Nanocomposite Monolith for Gamma Scintillation. *ACS Nano,* 11(6), 6422-6430.

Liu, D., Pourrahimi, A. M., Olsson, R. T., Hedenqvist, M. S., & Gedde, U. W. (2015). Influence of nanoparticle surface treatment on particle dispersion and interfacial adhesion in low-density polyethylene/aluminium oxide nanocomposites. *European Polymer Journal,* 66(Supplement C), 67-77.

Liu, D. Y., Yuan, X. W., Bhattacharyya, D., & Easteal, A. J. (2010). Characterisation of solution cast cellulose nanofibre - Reinforced poly(lactic acid). *Express Polymer Letters* 4(1), 26-31.

Liu, Y., Sun, D., Askari, S., Patel, J., Macias-Montero, M., Mitra, S., . . . Maguire, P. (2015). Enhanced Dispersion of TiO2 Nanoparticles in a TiO2/PEDOT:PSS Hybrid Nanocomposite via Plasma-Liquid Interactions. *Scientific Reports,* 5, 15765.

Medina-Esquivel, R., Freile-Pelegrin, Y., Quintana-Owen, P., Yáñez-Limón, J. M., & Alvarado-Gil, J. J. (2008). Measurement of the Sol–Gel Transition Temperature in Agar. *International Journal of Thermophysics,* 29(6), 2036.

Moon, R. J., Martini, A., Nairn, J., Simonsen, J., & Youngblood, J. (2011). Cellulose nanomaterials review: structure, properties and nanocomposites. *Chem Soc Rev,* 40(7), 3941-3994.

Müller, K., Bugnicourt, E., Latorre, M., Jorda, M., Echegoyen Sanz, Y., Lagaron, J. M., . . . Schmid, M. (2017). Review on the Processing and Properties of Polymer Nanocomposites and Nanocoatings and Their Applications in the Packaging, Automotive and Solar Energy Fields. *Nanomaterials,* 7(4), 74.

Nogi, M., Iwamoto, S., Nakagaito, A. N., & Yano, H. (2009). Optically Transparent Nanofiber Paper. *Advanced Materials,* 21(16), 1595-1598.

Oun, A. A., & Rhim, J.-W. (2015). Effect of post-treatments and concentration of cotton linter cellulose nanocrystals on the properties of agar-based nanocomposite films. *Carbohydrate Polymers,* 134(Supplement C), 20-29.

Pandey, N., Shukla, S. K., & Singh, N. B. (2017). Water purification by polymer nanocomposites: an overview. *Nanocomposites,* 3(2), 47-66.

Parker, R. M., Frka-Petesic, B., Guidetti, G., Kamita, G., Consani, G., Abell, C., & Vignolini, S. (2016). Hierarchical Self-Assembly of Cellulose Nanocrystals in a Confined Geometry. *ACS Nano,* 10(9), 8443-8449.

Petersson, L., Kvien, I., & Oksman, K. (2007). Structure and thermal properties of poly(lactic acid)/cellulose whiskers nanocomposite materials. *Composites Science and Technology,* 67(11-12), 2535-2544.

Qiang, X., Chunfang, Z., JianZun, Y., & Yuan, C. S. (2004). The effects of polymer-nanofiller interactions on the dynamical mechanical properties of PMMA/CaCO3 composites prepared by microemulsion template. *Journal of Applied Polymer Science,* 91(5), 2739-2749.

Rahman, I. A., Vejayakumaran, P., Sipaut, C. S., Ismail, J., & Chee, C. K. (2008). Effect of the drying techniques on the morphology of silica nanoparticles synthesized via sol–gel process. *Ceramics International,* 34(8), 2059-2066.

Riggs, B. C., Adireddy, S., Rehm, C. H., Puli, V. S., Elupula, R., & Chrisey, D. B. (2015). Polymer Nanocomposites for Energy Storage Applications. *Materials Today: Proceedings,* 2(6), 3853-3863.

Rusli, R., & Eichhorn, S. J. (2008). Determination of the stiffness of cellulose nanowhiskers and the fiber-matrix interface in a nanocomposite using Raman spectroscopy. *Applied Physics Letters,* 93(3), 033111-033113.

Sahoo, N. G., Rana, S., Cho, J. W., Li, L., & Chan, S. H. (2010). Polymer nanocomposites based on functionalized carbon nanotubes. *Progress in Polymer Science,* 35(7), 837-867.

Santamaria-Echart, A., Ugarte, L., Gonzalez, K., Martin, L., Irusta, L., Gonzalez, A., . . . Eceiza, A. (2017). The role of cellulose nanocrystals incorporation route in waterborne polyurethane for preparation of electrospun nanocomposites mats. *Carbohydrate Polymers,* 166(Supplement C), 146-155.

Schott, H. (1992). Swelling kinetics of polymers. *Journal of Macromolecular Science, Part B,* 31(1), 1-9.

Segal S., C. J. J., Martin A.E., Conrad C.M. . (1959). An empirical method of estimating the degree of crystallinity of native cellulose using the X-ray diffractometer. *Textile Research Journal,* 29, 786-794.

Shumigin, D., Tarasova, E., Krumme, A., & Meier, P. (2011). Rheological and Mechanical Properties of Poly(lactic) Acid/Cellulose and LDPE/Cellulose Composites. *MATERIALS SCIENCE (MEDŽIAGOTYRA),* 17(1), 32-37.

Tematio, C., Fosso, N., Krähenbühl, J., & Schintke, S. (2016). Conductive polymer nanocomposites for transparent circuits and thin films. *2016 18th International Conference on Transparent Optical Networks (ICTON)* (pp. 1-5).

Trache, D., Hussin, M. H., Haafiz, M. K. M., & Thakur, V. K. (2017). Recent progress in cellulose nanocrystals: sources and production. *Nanoscale,* 9(5), 1763-1786.

Trivedi, T. J., Rao, K. S., & Kumar, A. (2014). Facile preparation of agarose-chitosan hybrid materials and nanocomposite ionogels using an ionic liquid via dissolution, regeneration and sol-gel transition. *Green Chemistry,* 16(1), 320-330.

Wang, W., Wang, J., Kang, Y., & Wang, A. (2011). Synthesis, swelling and responsive properties of a new composite hydrogel based on hydroxyethyl cellulose and medicinal stone. *Composites Part B: Engineering,* 42(4), 809-818.

Wang, Z., Zhang, R., Ma, Y., Peng, A., Fu, H., & Yao, J. (2010 a). Chemically responsive luminescent switching in transparent flexible self-supporting [EuW10O36]9--agarose nanocomposite thin films. *Journal of Materials Chemistry,* 20(2), 271-277.

Wang, Z., Zhang, R., Ma, Y., Zheng, L., Peng, A., Fu, H., & Yao, J. (2010 b). Transparent and flexible phosphomolybdate-agarose composite thin films with visible-light photochromism. *Journal of Materials Chemistry,* 20(6), 1107-1111.

Weimer, P. J., Hackney, J. M., & French, A. D. (1995). Effects of chemical treatments and heating on the crystallinity of celluloses and their implications for evaluating the effect of crystallinity on cellulose biodegradation. *Biotechnology and Bioengineering,* 48(2), 169-178.

Xiaodong, L., Hongsheng, G., Wally, A. S., Dongling, F., Vivek, T., Michael, A. S., . . . Michael, L. M. (2005). Structural and mechanical characterization of nanoclay-reinforced agarose nanocomposites. *Nanotechnology,* 16(10), 2020.

Xu, X., Liu, F., Jiang, L., Zhu, J. Y., Haagenson, D., & Wiesenborn, D. P. (2013). Cellulose Nanocrystals vs. Cellulose Nanofibrils: A Comparative Study on Their Microstructures and Effects as Polymer Reinforcing Agents. *ACS Applied Materials & Interfaces,* 5(8), 2999-3009.

Yang, H., Liang, T., Qi, X., Jiang, H., Deng, Y., Wang, P., & Gao, H. (2017). Solvothermal synthesis of hydroxyapatite nanorods with assistance of green polymer. *Materials Science and Engineering: C,* 79(Supplement C), 9-14.

Yu, H.-Y., Zhang, H., Song, M.-L., Zhou, Y., Yao, J., & Ni, Q.-Q. (2017). From Cellulose Nanospheres, Nanorods to Nanofibers: Various Aspect Ratio Induced Nucleation/Reinforcing Effects on Polylactic Acid for Robust-Barrier Food Packaging. *ACS Applied Materials & Interfaces,* 9(50), 43920-43938.

Zakir Hossain, K. M., Jasmani, L., Ahmed, I., Parsons, A. J., Scotchford, C. A., Thielemans, W., & Rudd, C. D. (2012). High cellulose nanowhisker content composites through cellosize bonding. *Soft Matter,* 8(48), 12099-12110.

Zare, Y., & Shabani, I. (2016). Polymer/metal nanocomposites for biomedical applications. *Materials Science and Engineering: C,* 60(Supplement C), 195-203.